

Cite this: *Nanoscale Horiz.*, 2023, 8, 1700Received 16th August 2023,  
Accepted 5th October 2023

DOI: 10.1039/d3nh00363a

rsc.li/nanoscale-horizons

# A selenoureido-iminoglycolipid transported by zeolitic-imidazolate framework nanoparticles: a novel antioxidant therapeutic approach†

Fátima Guerrero,<sup>a</sup> Andrés Carmona,<sup>id</sup><sup>a</sup> Victoria Vidal,<sup>a</sup> Ana Franco,<sup>id</sup><sup>b</sup>  
Alejandro Martín-Malo,<sup>a</sup> Elena M. Sánchez-Fernández<sup>\*c</sup> and  
Carolina Carrillo-Carrión<sup>id</sup><sup>\*d</sup>

A selenium-containing metal–organic framework with remarkable antioxidant capacity and ROS-scavenging activity was constructed by a controlled *de novo* encapsulation approach of a glycoconjugate mimetic, specifically a sp<sup>2</sup>-iminoglycolipid bearing a selenoureido fragment (DSeU), within a zeolitic-imidazolate framework exoskeleton. Biocompatible and homogeneous nanosized particles of ~70 nm (DSeU@ZIF8) were obtained, which could be efficiently internalized in cells, overcoming the poor solubility in biological media and limited bioavailability of glycolipids. The ZIF-particle served as nanocarrier for the intracellular delivery of the selenocompound to cells, promoted by the acidic pH inside endosomes/lysosomes. As demonstrated by *in vitro* studies, the designed DSeU@ZIF8 nanoparticles displayed a high antioxidant activity at low doses; lower intracellular ROS levels were observed upon the uptake of DSeU@ZIF8 by human endothelial cells. Even more interesting was the finding that these DSeU@ZIF8 particles were able to reverse to a certain level the oxidative stress induced in cells by pre-treatment with an oxidizing agent. This possibility of modulating the oxidative stress in living cells may have important implications in the treatment of diverse pathological complications that are generally accompanied with elevated ROS levels.

## New concepts

Reactive oxygen species (ROS) are vital for cell functions; however, high ROS levels are associated with diverse pathologies. This fact highlights the relevance of developing therapeutic tools capable of regulating ROS. In this direction, we report a selenium-containing metal–organic framework endowed with intracellular antioxidant and ROS-scavenging properties. The nanoplatform design relies on combining (1) a glycomimetic bearing a selenoureido fragment, presenting antioxidant capacity (not investigated yet), and (2) the exceptional features of zeolitic-imidazolate framework-8 (ZIF8) to encapsulate and carry biomacromolecules into cells, while allowing for a controlled pH-mediated release. Previous efforts have been made on incorporating carbohydrates into ZIF8. However, as with other biomacromolecules, achieving a good synthetic control is not a simple task, as revealed the reported results so far. Importantly, we have successfully developed a precise encapsulation strategy, resulting in homogeneous and reproducible DSeU@ZIF8 nanoparticles; key to ensuring subsequent reproducible and reliable cellular responses. Equally important, we have demonstrated that DSeU@ZIF8 were capable of modulating the basal ROS level in endothelial cells, could mitigate the H<sub>2</sub>O<sub>2</sub>-induced cell damage and had also a beneficial impact on preserving critical endothelial functions. These results may serve as inspiration for innovative nanotherapies in the treatment of pathologies associated with oxidative stress.

## Introduction

The effect of reactive oxygen species (ROS) is a double-edged sword due to its dual function. While moderate ROS levels are vital for cell signalling and intracellular functions, a high ROS

production is detrimental, capable of depleting the antioxidant enzymatic tool, and, eventually, inducing cell death.<sup>1</sup> Indeed, elevated ROS levels are associated with very diverse pathologies, including inflammatory, neurodegenerative, respiratory and cardiovascular diseases, as well as different types of cancer.<sup>2</sup> Accumulating research in the last decades highlights the role that ROS plays as mediators in the activation of transcription factors, intracellular signaling pathways (*e.g.* nuclear factor-kappa B (NF-κB), mitogen-activated protein kinase (MAPK) cascade) and in the immune response.<sup>3</sup> Glutathione peroxidase (GPx), a well-known human selenoprotein containing a selenocysteine residue in its active site, is one of the key antioxidant enzymes responsible for the balance of oxidative stress in cells under physiological conditions. GPx effectively reduces hydrogen peroxide (H<sub>2</sub>O<sub>2</sub>) and lipid peroxides, preventing thus cells from damage caused by these oxidant species.<sup>4</sup> It is not a

<sup>a</sup> Maimonides Biomedical Research Institute of Cordoba (IMIBIC), Reina Sofia University Hospital, 14004 Córdoba, Spain

<sup>b</sup> Leibniz Institute für Katalyse e. V., 18059 Rostock, Germany

<sup>c</sup> Department of Organic Chemistry, Faculty of Chemistry, University of Seville, C/ Profesor García González 1, 41012 Sevilla, Spain. E-mail: esanchez4@us.es

<sup>d</sup> Institute for Chemical Research (IIQ), CSIC-University of Seville, Avda. Américo Vespucio 49, 41092 Sevilla, Spain. E-mail: carolina.carrillo@csic.es

† Electronic supplementary information (ESI) available: Full experimental procedures, characterization details, and additional supporting data and figures. See DOI: <https://doi.org/10.1039/d3nh00363a>



coincidence that nature has chosen selenium due to its unique ability to react with oxygen and related ROS in a readily reversible manner, being able to both rapidly become oxidized and then be rapidly reduced (referred to as the “selenium paradox”).<sup>5</sup> To mimic the intracellular GPx antioxidant activity, some organoselenium compounds<sup>6</sup> and selenium (Se)-containing nanomaterials<sup>7</sup> have been investigated with pharmacological purposes.

Within the field of carbohydrates, several Se-based sugars have been reported to date with relevant biological properties.<sup>8</sup> Among them, a few *N*-glycosides merging in their structures the widely studied organic seleno compound Ebselen,<sup>9</sup> which features a selenenylamide group, stand out with improved antimetastatic properties.<sup>10</sup> Likewise, some synthetic strategies have been implemented to install the Se atom or related functionalities (*i.e.*, selenocarbamates, selenoureas) as glycosidic linkages, providing Se-based glycosides chemically and enzymatically more resistant.<sup>11</sup>

In this scenario, Se-bearing  $sp^2$ -iminoglycolipids ( $sp^2$ -IGLs) have been recently reported by our research group displaying enhanced abilities as context-dependent regulators of the immune system compared to their bioisosteric S-containing counterparts:  $sp^2$ -iminosugar selenoglycolipids<sup>12</sup> and  $sp^2$ -glycosylselenoureas.<sup>13</sup> This family of stable and functional glycomimetics derived from the natural iminosugar nojirimycin features as glycone core a cyclic pseudoamide-type function ( $sp^2$ -hybridation) replacing the endocyclic nitrogen atom,<sup>14</sup> compatible with the incorporation of O-, N-, C-, S-, Se-containing  $\alpha$ -oriented aglyconic substituents.<sup>12,15</sup> Structure–activity relationship studies of the generated library of glycolipid mimetics have revealed that linear aliphatic chains of twelve carbon atoms ( $C_{12}$  vs.  $C_4/C_8/Ph$ ) usually lead to better pharmacological activities covering multiple scenarios (*e.g.*, parasitic infections, a variety of cancers, and inflammatory diseases such as diabetic retinopathy and nephropathy).<sup>16</sup> Focused on this scenario, further advances have been achieved with the  $\alpha$ -dodecylselenoureido-glycoside (referred to as DSeU, Fig. 1(A)) bearing a selenourea-type linkage at the pseudoanomeric position of the nojirimycin derivative. Previous works with DSeU showed a prominent anti-inflammatory response both *in vitro* (LPS-treated murine splenocytes) and *in vivo* systems (animal model of airway hyper-reactivity triggered by ovalbumin), evidencing its potential as drug candidate against immune-related disorders.<sup>13</sup> Surprisingly, despite the remarkable findings of DSeU in inflammatory processes and the close relationship between oxidative stress and chronic inflammation,<sup>17</sup> the potential antioxidant function of DSeU has not been explored yet.

On the other hand, a major bottleneck common to all the  $sp^2$ -IGLs is their low solubility in biological media and consequent limited bioavailability, which is most likely the reason why the full therapeutic potential of these compounds is still under-exploited. Doses around 10–50  $\mu$ M are required to observe a significant cellular response both *in vitro*,<sup>18</sup> *ex vivo*<sup>19,20</sup> and *in vivo* models.<sup>13,21</sup> This suggests that  $sp^2$ -IGLs are not efficiently internalized into cells, either due to their inactivation (by aggregation/insolubilization) in the extracellular medium before reaching the cell interior or by the sluggish diffusion across the cell membrane. We envision that this obstacle could be overcome by encapsulating these immunoregulatory  $sp^2$ -IGL

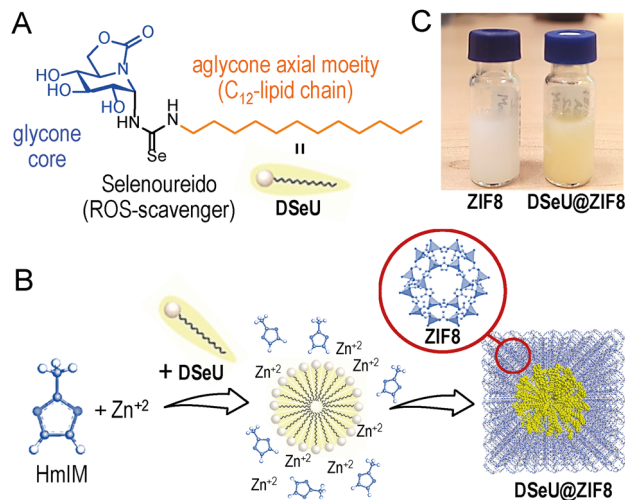


Fig. 1 (A) Chemical structure of DSeU, selected as lead compound. (B) Schematic representation of the one-pot synthesis of DSeU@ZIF8 particles, showing the plausible mechanism of formation proposed. The crystal structure of ZIF8 with the sodalite framework topology is also shown. (C) Photographs of the resulting suspensions of the DSeU@ZIF8 and control ZIF8 particles (specifically ZIF8/Cnt2) after purification.

agents into nanomaterials that act as nanocarriers to efficiently solubilize and transport them into cells.

Among the wide variety of nanomaterials used as nanocarriers, metal–organic frameworks (MOFs), coordination networks of metal ions or clusters linked by polydentate organic ligands resulting in materials with potential voids,<sup>22</sup> have already demonstrated their superior performance as drug delivery systems (DDSS) compared to conventional porous nanomaterials.<sup>23</sup> This is due to their high compositional/structural tuneability, as well as the possibility to control their particle size,<sup>24</sup> internal porosity,<sup>25</sup> and surface chemistry.<sup>26</sup> With the aim of encapsulating large biomolecules, zeolitic-imidazolate frameworks (ZIFs, a subfamily of MOFs built with tetrahedral metal ions and imidazoles) are of particular interest, being the ZIF-8 the most used for two reasons: (i) its high biocompatibility and minimal toxicity; and (ii) it allows a pH-controlled release of the encapsulated cargo due to the decomposition of the ZIF-8 matrix at pH values  $\leq 6.5$  or in specific buffer solutions (*e.g.*, phosphate buffered saline (PBS)).<sup>27</sup> In this line, several researchers have recently reported the efficient encapsulation of biomacromolecules, including proteins, nucleic acids and glycosaminoglycans, into ZIFs through a process termed biomimetic mineralization, in which the MOF precursors self-assemble around the biomolecule encapsulating it within a porous crystalline matrix.<sup>28</sup> Notably, the MOF matrix serves as a protective coating in case of fragile or environment-sensitive biomolecules, preventing thus the loss of their biological activity before reaching the target action site, and also acts as a vector for enhancing the intracellular delivery of the active biomolecule. Despite the advances in the synthetic approaches for the preparation of biomolecules@MOF composites, the lack of control in the number of biomolecules loaded per MOF particle and their spatial distribution within the framework is still the main issue to be solved, which is likely hindering the



translation of these therapeutic nanoplatfroms from bench to clinic.

Within the context of glyco-MOFs, some interesting works have reported the functionalization of the MOF surface with carbohydrates (*e.g.*, glycopolymers, maltose-containing surfactants) for targeting purposes.<sup>29</sup> Attempts to use carbohydrates as building units for the construction of MOFs have also been carried out, but to date only cyclodextrins (CDs), have led to the formation of CD-MOF crystals.<sup>30</sup> Surprisingly, the encapsulation of carbohydrates in MOFs has been pushed aside for a long time, until very recently Falcaro *et al.* have developed a strategy for the encapsulation of glycosaminoglycans<sup>31</sup> (GAGs, *i.e.*, high-molecular weight polysaccharides) in three ZIFs types with different pH-responsiveness to modulate the release profiles of the encapsulated biopolymer. It is worth noting that, so far, the formation of carbohydrate@MOF composites has been prepared only with GAGs, a clear indication that the glyco-MOF field is still in its infancy. Indeed, this work clearly demonstrated that the formation of such composites is not a simple task, obtaining generally particles that are not homogeneous in size, with some aggregation, and in some cases with mixtures of different crystalline phases.<sup>31</sup>

Herein, we set out to explore the therapeutic potential of a Se-containing sp<sup>2</sup>-IGL, the aforementioned DSeU (Fig. 1(A)), as an antioxidant agent using ZIF8 as DDS for its efficient transport and subsequent pH-triggered intracellular delivery. This strategy might lead to a higher accumulation of the seleno-sp<sup>2</sup>-iminosugar inside cells, resulting in a superior antioxidant activity promoted by the reduction of the intracellular ROS levels. To this aim, we faced first the challenge of incorporating the glyco-compound inside a ZIF structure in a controlled and reproducible manner, to prepare homogeneous DSeU@ZIF8 nanoparticles (even between different batches), the key to ensuring subsequent reproducible and reliable cellular responses. Afterwards, we performed *in vitro* studies to evaluate the antioxidant activity and ROS-scavenging properties of the as-designed nanoparticles, together with functional assays to demonstrate its biocompatibility at the therapeutic concentrations used and to investigate the possible recovery of lost endothelial functions after subjecting cells to oxidative treatments.

## Results and discussion

Considering the aforementioned *in vitro* and *in vivo* therapeutic immunomodulatory properties of DSeU<sup>13</sup> and the well-known role played by the selenoureido motif as ROS scavenging,<sup>32</sup> we selected this bioactive sp<sup>2</sup>-IGL as target candidate to perform the proof-of-concept study. The stereoselective synthesis of (1*S*)-(N'-dodecylselenoureido)-5*N*,6*O*-oxomethylidenenojirimycin<sup>13</sup> (DSeU, Fig. 1(A)) was accomplished from (1*R*)-1,2,3,4-tetra-*O*-acetyl-5*N*,6*O*-oxomethylidenenojirimycin<sup>14</sup> in a synthetic sequence of five steps (see ESI† for details, Fig. S1–S6). Briefly, the synthetic procedure involves the  $\alpha$ -glycosyl isothiocyanate as precursor of the protected  $\alpha$ -dodecylthiourea, which through a process of oxidative desulfurization led to the corresponding  $\alpha$ -glycosyl-carbodiimide. The procedure reported by Koketsu, Ishihara

*et al.*<sup>33</sup> using the selenating reagent LiAlHSeH (generated *in situ*) allowed the incorporation of the selenoureido fragment in the sp<sup>2</sup>-IGL. Further conventional de-*O*-acetylation reaction successfully afforded DSeU. Afterwards, DSeU@ZIF8 nanoparticles were synthesized under mild conditions (in water and at room temperature) *via* one-pot process by mixing aqueous solutions of the ZIF8 precursors, that is Zn(NO<sub>3</sub>)<sub>2</sub> and 2-methylimidazole (HmIM), followed by the addition of a methanolic solution of DSeU under gentle stirring (Fig. 1(B)). The mixture was then left undisturbed for 2 h, and the gradual appearance of a yellowish/orange turbidity was observed during this time, indicative of the formation of DSeU@ZIF8 particles. After purification, particles were redispersed in methanol (Fig. 1(C)) for long-term storage at 4 °C, and diluted in water or cell culture medium just before use. Following this procedure, sp<sup>2</sup>-IGLs are incorporated during the synthesis of the ZIF8 crystals, which is referred to as *de novo* or biomimetic mineralization encapsulation approach.

The plausible mechanism for the formation of the DSeU@ZIF8 particles is likely the directed crystallization of ZIF around the preformed micelles of DSeU, being thus the amphiphilic/surfactant-like character of sp<sup>2</sup>-IGLs a key feature in the process. The aqueous phase synthesis (water:methanol, 10:1) guarantees the formation of DSeU micelles, whereas the multiple hydroxyl groups present on the glycone core of the DSeU may provide the anchoring to bridge Zn(HmIM)<sub>2</sub> clusters and micelles. Experimental parameters such as the ratio of precursors, solvent and growth time (Table S1, ESI†), were optimized to maximize the encapsulation efficiency (EE%) and to obtain homogeneous particles with an average size <100 nm; note that MOF particles smaller than ~100–150 nm usually leads to higher internalization rates by cells. The EE% was determined by high-performance liquid chromatography (HPLC) quantification of the non-encapsulated DSeU (remaining in the supernatant after purification of the particles by centrifugation). It is worth noting that achieving a high EE% is very relevant in this application as the therapeutic DSeU agent is the valuable component of the DSeU@ZIF8 composite, whereas the cost of the ZIF8 precursors is almost negligible comparatively. Importantly, we found that the DSeU concentration was critical for the successful formation of DSeU@ZIF8 particles (Fig. S7 and Table S1, ESI†), suggesting that the control in the process relies on the proper formation of DSeU micelles and supporting the hypothesis that these micelles act as nucleation seeds for the further growth of a ZIF8 shell around. At low DSeU concentrations (<0.2 mM) we were unsuccessful in incorporating DSeU molecules into the ZIF particle in an efficient manner, but notably the morphology of the particles (size and shape) was significantly different from the ZIF8 control sample. This finding indicates that DSeU is capable of acting as a size/shape-controlling agent, just as reported for other surfactant molecules such as cetyltrimethylammonium bromide (CTAB).<sup>34</sup> When using a concentration of 0.9 mM, at which the compound is mostly as micelles, quite homogenous DSeU@ZIF8 particles were achieved, containing on average one micelle per particle along with an almost quantitative encapsulation, so that this concentration was



fixed as the optimal. It corresponds to an amount of 6  $\mu\text{mol}$  of DSeU per synthesis. A further increase in the concentration resulted in particles containing several micelles of compound inside each particle, and thus without control in the number of micelles per particle (Fig. S7, ESI<sup>†</sup>). It is of special relevance to highlight the exceptional synthetic control achieved in this work for the preparation of ZIF8 nanoparticles incorporating a glycolipid mimetic in a very efficient way. We must keep in mind that a precise control in the synthesis that leads to homogeneous particles will be decisive in having reliable and reproducible biological results. Regarding the growth time, the changes on the hydrodynamic diameter ( $d_h$ ) of the particles over time were monitored by dynamic light scattering (DLS). The results showed a fast initial kinetics, reaching a size of  $\sim 50$  nm after 30 min; then the growth slowed down while an improvement in the homogeneity of the particles was observed (lower polydispersity index, PdI). After 2 h, the size of the particles hardly changed (Fig. S8, ESI<sup>†</sup>). Under the final optimized experimental conditions (0.59 M of HmIM, 11.4 mM of  $\text{Zn}^{2+}$ , 0.91 mM of DSeU, 10:1  $\text{H}_2\text{O}:\text{MeOH}$ , 2 h; Table S1, ESI<sup>†</sup>), the EE% and loading capacity (LC%) were found to be 97% and 5.8 wt%, respectively, as determined by HPLC analyses (see ESI<sup>†</sup> for details). These values are of the same order as those reported for similar systems (*i.e.*, biomolecules in ZIFs).<sup>28d</sup>

Regarding the structural features of the resulting DSeU@-ZIF8 particles, they had a size of  $\sim 70$  nm and a cubic shape

with rounded edges as determined by transmission electron microscopy (TEM), Fig. 2(A), (B) and Fig. S10 (ESI<sup>†</sup>). Scanning electron microscopy coupled with energy-dispersive X-ray spectroscopy (SEM-EDX) analysis was used to analyse the composition of the particles, showing the presence of N coming from the HmIM ligands and the peaks corresponding to Se and Zn atoms (Se/Zn ratio = 0.072), which confirmed the incorporation of DSeU molecules within the ZIF8 (Fig. S11, ESI<sup>†</sup>). It is interesting to note that micelles were located in the centre of the ZIF structure, as shown in TEM images (Fig. 2(B)), which support again the hypothesis that these micelles acted as seeds for the subsequent formation of a ZIF8 shell around them, as previously mentioned. Comparison of the morphology of DSeU@ZIF8 with two types of ZIF8 particles synthesized as controls (Fig. S9 and S10, ESI<sup>†</sup>), one replacing the  $\text{sp}^2$ -IGL solution by methanol (ZIF8/Cnt1) and the other using CTAB instead of the  $\text{sp}^2$ -IGL (ZIF8/Cnt2; shown in Fig. 1(C)), further confirmed the ability of the glycolipids to modulate the growth of the ZIF structure. In a biological context, comparing the behavior of particles with very different sizes makes no sense, since it is well known that size is one of the determining factors in the pathway and kinetics of cellular uptake.<sup>35</sup> Therefore, we decided to use the ZIF8/Cnt2 sample as control particles (denoted from now on as ZIF8), having a size of  $\sim 100$  nm, which is quite similar to the DSeU@ZIF8.

To investigate the successful encapsulation of the DSeU, we performed  $^1\text{H}$  nuclear magnetic resonance ( $^1\text{H}$  NMR) analyses

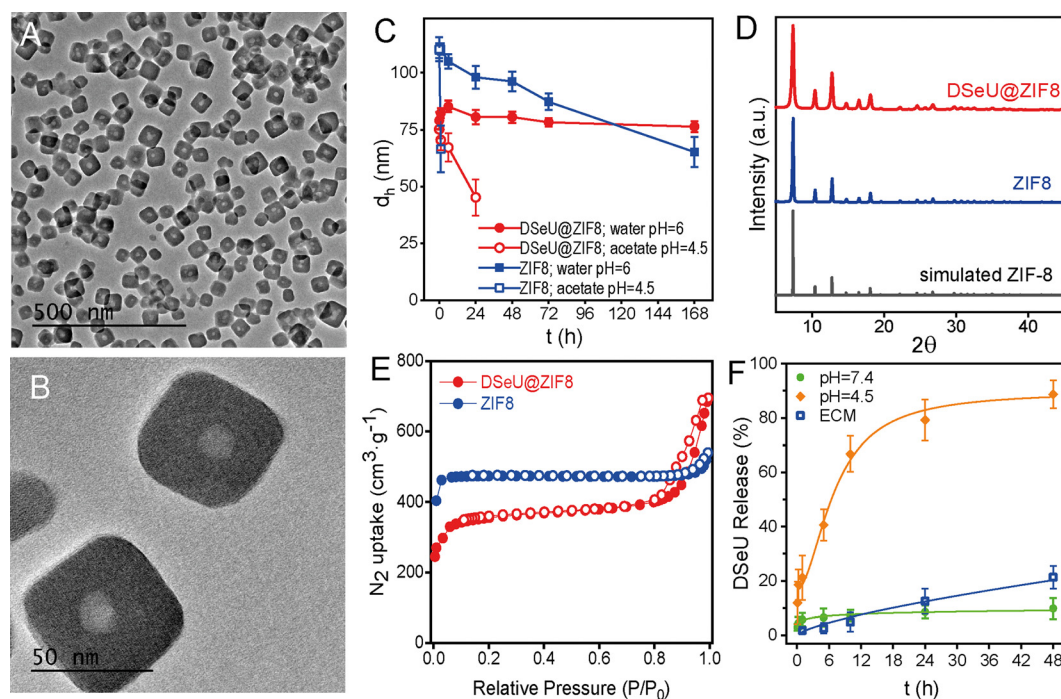


**Fig. 2** (A) and (B) Representative TEM images at different magnifications of DSeU@ZIF8 particles. (C) Colloidal stability over time of the DSeU@ZIF8 and control ZIF8 particles dispersed in either Milli-Q water (pH  $\sim 6.0$ ) or acid medium (acetate buffer solution, pH = 4.5), as determined by DLS. Data are shown as mean  $\pm$  SD,  $n = 3$  independent replicates. (D) PXRD patterns of DSeU@ZIF8 and ZIF8 particles, as well as the simulated ZIF8 calculated from cif.file (COD (Crystallography Open Database): 7111970) for comparison. (E)  $\text{N}_2$  isotherms (77 K) of DSeU@ZIF8 and ZIF8 particles. Closed symbols represent adsorption, and empty symbols represent desorption. (F) Kinetic profiles of DSeU released from the DSeU@ZIF8 particles dispersed in two different pH media and in endothelial cell culture media (ECM), as determined by HPLC quantification. Data are shown as mean  $\pm$  SD,  $n = 3$  independent replicates. Note that experiments in ECM at the first time points (5 and 15 min) were below the limit of quantification (LOQ) of the HPLC method.



of the free DSeU, the DSeU@ZIF8 particles dispersed in CD<sub>3</sub>OD (*i.e.*, colloidal suspension and perfectly stable during the NMR measurement), and after dissolving the particles by treatment with diluted acid due to the break of Zn–N bonds (Fig. S12, ESI†). The absence of characteristic signals of free DSeU in the <sup>1</sup>H NMR spectrum of DSeU@ZIF8 suggested that the selenourido derivative is trapped into the crystalline structure (and not simply adsorbed on the surface of the ZIF particle). Being confined in a solid and rigid structure, the protons of DSeU cannot resonate when applying the magnetic field. However, DSeU@ZIF8 showed two peaks at  $\delta$  6.88 and  $\delta$  2.37 ppm corresponding to aromatic C–H protons and CH<sub>3</sub> protons of the HmIM, respectively. On the other hand, when the DSeU@ZIF8 structure was destroyed under the presence of acids, the <sup>1</sup>H NMR spectrum of the resulting mixture showed the appearance of signals corresponding to the DSeU. This experimental data confirms that these sp<sup>2</sup>-IGLs were inside the DSeU@ZIF8 framework, and that the structure of the DSeU was preserved during their encapsulation and following delivering under acidic conditions, an essential requirement to later exploit their biological function once released in the cells.

Regarding the behavior of the DSeU@ZIF8 particles in solution, DLS measurements of the particles dispersed in water showed a very similar hydrodynamic size ( $d_h \sim 80$  nm) as that shown in methanol, as well as a low PDI, which is indicative of a homogenous population of particles (Fig. S13 and Table S2, ESI†). The  $\zeta$ -potential value of the DSeU@ZIF8 in Milli-Q water was determined to be *ca.* 12 mV; almost identical to that of the control ZIF8 particles (11.2 mV, Table S2, ESI†), suggesting that the sp<sup>2</sup>-IGL are encapsulated within the ZIF8 structure and not adsorbed on the particle surface. The colloidal stability of the DSeU@ZIF8 particles in water was evaluated by monitoring changes in the size ( $d_h$ ) over time, and the results showed that the particles presented superior stability than the control ZIF8 (Fig. 2(C) and Table S4, ESI†), ensuring thus the integrity of particles (present as individual particles and not aggregated or dissolved quickly) for long enough to be uptaken by cells in a considerable extent. This fact was also clearly observable by visual inspection, given the different rate of turbidity loss of both particle's suspensions. Going a step further, we investigated if the chemical stability of DSeU@ZIF8 was also enhanced compared to the pristine ZIF8 under unfavorable conditions, specifically in acid medium. For that, DSeU@ZIF8 and ZIF8 particles were suspended in acid medium (acetate buffer solution at pH = 4.5 prepared in D<sub>2</sub>O), and the amount of HmIM released to the medium was monitored by <sup>1</sup>H NMR (Fig. S14 and S15), see ESI† for details. The results showed that ZIF8 was degraded quickly as expected (86% of HmIM released in 6 h), while the degradation of the DSeU@ZIF8 particles was significantly slower (only 24% after 6 h, and 63% after 24 h, Fig. S16 (ESI†)). These findings are consistent with a previous report that demonstrated a symbiotic stability reinforcement effect between bioentities (enzymes and DNA) and ZIF8.<sup>36</sup> In this work we have proven that this stabilizing effect is also extensible to glycolipids; *i.e.*, the encapsulated biomolecules stabilize the ZIF matrix while the ZIF exoskeleton protects the biomolecule from denaturation or degradation.

Next, powder X-ray diffraction (PXRD) revealed that the DSeU@ZIF8 was crystalline, showing the characteristic Bragg peaks of the typical sodalite (sod) structure of ZIF8, matching well with the simulated XRD pattern (Fig. 2(D)). Slight changes in the intensity and broadening of some peaks in the pattern of DSeU@ZIF8 compared to that of ZIF8 particles may be attributed to the smaller size of the DSeU@ZIF8 particles, as well as to the presence of some structural defects within the framework due to the incorporation of DSeU micelles, which also served as evidence that the compound is indeed into the particles. Additionally, we conducted N<sub>2</sub> uptake experiments to determine the effect of the encapsulation of DSeU on the porosity of the ZIF particles. While ZIF8 particles presented a reversible type I isotherm, typical for microporous materials, DSeU@ZIF8 displayed type I/type IV isotherms with a hysteresis loop at high relative pressures, suggesting the presence of mesoporous, which is consistent with the presence of the micelles into the ZIF8 framework (Fig. 2(E)). On the other hand, the isotherms of the DSeU@ZIF8 showed in principle a slight decrease in the Brunauer–Emmett–Teller area ( $S_{\text{BET}}$ ) and micropore volume ( $V_{\text{micro}}$ ) compared to the control ZIF8 (Table S3, ESI†). However, after correction considering exclusively the ZIF8 weight (Table S3, ESI†), we realized that the actual BET area of DSeU@ZIF8 was almost identical to that of the control ZIF8 particles, that is, the microporosity of the imidazolate framework is fully preserved. This finding once again supports the statement that the here proposed strategy for the DSeU@ZIF8 synthesis allows the incorporation of the selenocompound in a highly controlled manner in the centre of the particle and minimally affecting the rest of the ZIF matrix.

Afterwards, we tested the stability of the as-prepared DSeU@ZIF8 nanoparticles under biological relevant conditions. Taking into account that the Zn–N bond in ZIF8 is sensitive to phosphate ions, which are usually present in cell culture medium, the particles were incubated in endothelial cell culture medium (ECM) to study the potential degradation of the DSeU@ZIF8 particles in cell medium with the subsequent unwanted extracellular release of DSeU. For that, we determined the amount of DSeU released to the medium at different time points by HPLC, as an indirect way to investigate the particles degradation. The results revealed that the DSeU release was minimal during the first day in ECM (*ca.* 5% after 10 h and 12% after 24 h; Fig. 2(F)), ensuring that the particles preserve their structural integrity in the extracellular environment for long enough to be internalized into cells. We next studied the pH-responsiveness of these DSeU@ZIF8 nanoparticles in order to exploit the pH differences between cellular environments (extracellular *vs.* intracellular) as well as among healthy and diseased cells. Note that the pH in inflammatory tissues and in cancer cells is more acidic (in the range of  $\sim 4.5$ – $6.5$ )<sup>31,37</sup> that found in blood and healthy tissue ( $\sim 7.4$ ). Therefore, the DSeU@ZIF8 particles were incubated in two different pH media pH = 7.4 (Tris buffer solution) and pH = 4.5 (acetate buffer solution) for emulating those different cellular conditions, and we determined the release profiles by quantifying the amount of DSeU delivered to the medium as a function of time (see ESI† for details). As shown in Fig. 2(F),



there was a much higher release rate of DSeU at acidic condition (reaching 88.7% after 48 h) than those at the neutral condition (9.8% after 48 h), as expected according to the widely studied pH-dependent dissolution/degradation of ZIF8. Importantly, the release was fairly gradual in both cases, and any burst effect was observed, unlike to published results for ZIF-carbohydrates biocomposites (e.g., heparin release from ZIF8 at pH = 6 was ca. 70% within the first 5 min).<sup>31</sup> Note that the superior chemical stability in acidic media of the DSeU@ZIF8 compared to the pristine ZIF8, as discussed above (Fig. S14–S16, ESI†), is beneficial for achieving a slower sustained delivery of the therapeutic sp<sup>2</sup>-IGL, allowing thus a better control of the dose administration.

Once synthesized and characterized the DSeU@ZIF8 particles, we sought to explore their potential as antioxidant nano-platforms *via* ROS-scavenging. We selected human umbilical vein endothelial cells (HUVECs) as an appropriate *in vitro* model to assess the ROS-induced oxidative stress to endothelium. To choose the appropriate concentrations for cell assay, we first investigated the cytotoxicity of the free DSeU, ZIF8 and DSeU@ZIF8 particles by using two different cell viability assays (MTT and WST-1, see ESI† for details). Note that selecting an

optimal (low) concentration of the DSeU@ZIF8 and ZIF8 particles is critical to achieve an antioxidant effect, since it has been reported that high concentrations of ZIF-8, as for other MOF types, promote the ROS induction (due to metal leaching), with the consequent nanotoxicity.<sup>38</sup> As shown in Fig. 3(A) and (B), after exposure to increasing concentrations of the compound/particles (from 0 to 50 μM), cells showed the typical dose-dependent response. Note that the concentration of DSeU@ZIF8 (*c*, in μM) refers to the concentration of DSeU within the particles (considering that the amount of sp<sup>2</sup>-IGL encapsulated was 5.8 wt% as previously determined) to be able to directly compare the performance of the free and encapsulated DSeU as a function of the administered dose. Nevertheless, a second *x*-axis expressing the concentration of particles (*c*<sub>MOF</sub>, in μg mL<sup>-1</sup>) is also shown. Notably, the viability curves were comparable regardless of the assay used, ensuring thus the data reliability; therefore, we decided to use the WST-1 assay from now on to monitor the cell viability after the different treatments. Notably, besides the good cellular viability at these working concentrations, the cell morphology and adhesion were not affected in the presence of DSeU@ZIF8 particles, indicative of the biocompatibility of particles.

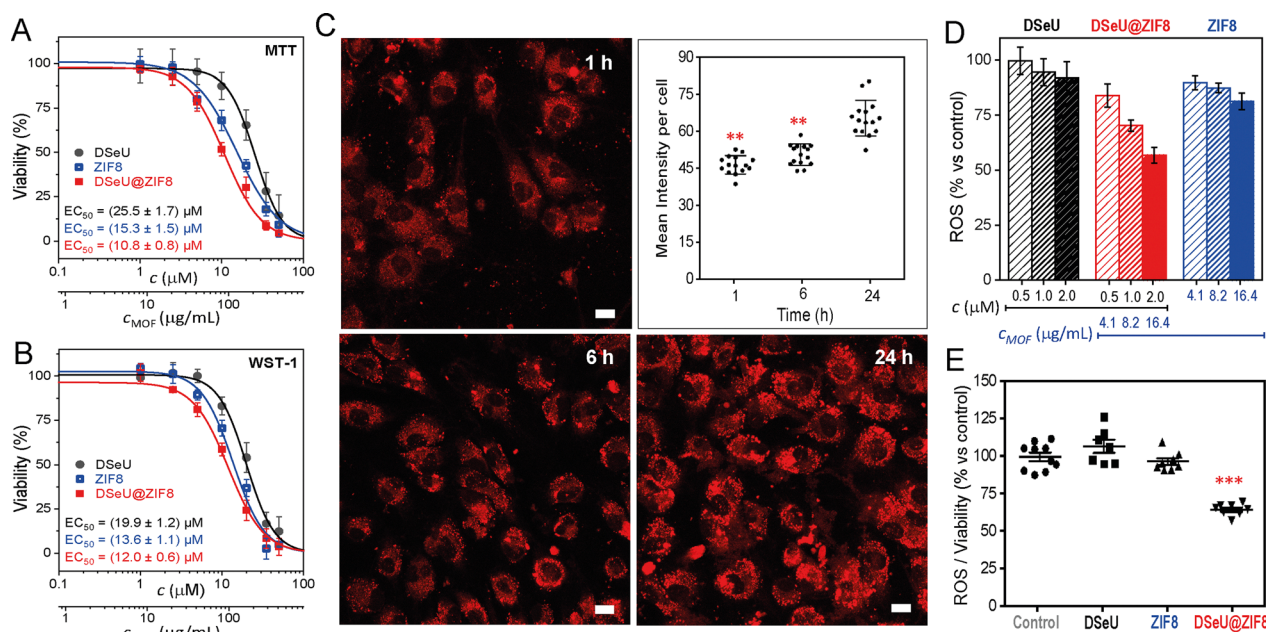


**Fig. 3** Cell viability of HUVEC cells under 24 h exposure to increasing concentrations of the different studied compound/particles as determined by (A) MTT assay and (B) WST-1 assay. *c* refers to the concentration of DSeU in μM, while *c*<sub>MOF</sub> corresponds to the particle concentration in μg mL<sup>-1</sup>. Half-maximal responses (EC<sub>50</sub> values) were calculated by fitting (logistic function in OriginLab, fixing minimum viability to 0%). (C) Cellular uptake of fluorescent RhB@DSeU@ZIF8 particles. Live-cells confocal microscopy images (40×) taken at different incubation times (1 h, 6 h and 24 h) of cells incubated with RhB@DSeU@ZIF8 particles (at a concentration of 8.2 μg mL<sup>-1</sup>), and showing the red fluorescence channel for RhB (λ<sub>ex</sub> = 514 nm, λ<sub>em</sub> = 575–650 nm). Scale bars correspond to 10 μm. Quantification of the uptake over time was done using the mean fluorescence intensity per cell (expressed as mean ± standard deviation with *n* = 15). *p* value < 0.05 was considered statistically significant; \*\**p* < 0.01 vs. 24 h. (D) Intracellular ROS (% vs. control) of cells incubated for 24 h with three doses of the compound/particles: *c* = 0.5, 1.0 and 2.0 μM of DSeU, or the equivalent particles concentration *c*<sub>MOF</sub> = 4.1, 8.2 and 16.4 μg mL<sup>-1</sup> for DSeU@ZIF8 and ZIF8, considering exclusively ZIF8 weight. Untreated cells are considered as control cells, from which the basal ROS level is determined. (E) Intracellular antioxidant capacity of DSeU@ZIF8 particles compared to that of the free administration of its counterparts (DSeU and ZIF8), as derived from the intracellular ROS generated in cells exposed 24 h to 1 μM (or equivalent 8.2 μg mL<sup>-1</sup> for particles) of the compound/particles. Data are normalized against the number of viable cells (*i.e.*, ROS content expressed as fluorescence intensity normalized against cell viability). Data are expressed as mean ± standard deviation with *n* = 3–10 independent replicates. *p* value < 0.05 was considered statistically significant; \**p* < 0.001 vs. control.



Next, cell uptake was also studied by loading the DSeU@ZIF8 particles with a fluorescent probe, specifically rhodamine B (see ESI† for details on the preparation of RhB@DSeU@ZIF8), with the aim of easily monitor the particles internalization in cells by confocal microscopy. The intracellular monitoring of the fluorescent RhB@DSeU@ZIF8 particles was carried at different incubation times (1 h, 6 h and 24 h). As shown in Fig. 3(C) and Fig. S17 (ESI†), the particles were internalized efficiently and with fairly rapid uptake kinetics, as a significant fluorescence signal per cell was found after only 1 h of incubation. Increasing the incubation time resulted in a greater cell uptake, as expected, with the cell being almost saturated with particles after 24 h. It is worth noting that the fluorescence appears punctuated (more easily observable at a magnification 63×, Fig. S18, ESI†), which indicates that the particles preserve their integrity when internalized. If they were degraded in the extracellular medium, the fluorescent probe (RhB) would be internalized as a free molecule and there would be a diffuse fluorescence signal throughout the cell, instead of the punctuated fluorescence pattern that is observed.

The effect of the DSeU@ZIF8 particles on the cellular oxidative state, in comparison with the free DSeU and the pristine ZIF8, was then investigated by incubating HUVEC cells for 24 h with three different doses of compound/particles by measuring the intracellular ROS level after each treatment (Fig. 3(D)). The range between 0.5–2 μM of DSeU (or the equivalent particles

concentration 4.1–16.4 μg mL<sup>-1</sup> for DSeU@ZIF8 and ZIF8) was selected to ensure a viability ≥ 90% for all the samples. The ROS level was determined by using 2,7-dichlorofluorescein-diacetate (DCFH-DA), a fluorescent indicator of the overall oxidation status of cells (see ESI† for details). With the aim of evaluating only the antioxidant activity inside cells, they were washed several times with PBS to remove the fraction of compound/particles not internalized. Also, untreated cells were used as a control to determine the basal ROS level. It is worth noting that keeping the basal level of ROS, above cytostatic but below cytotoxic levels, is vital for proper ROS or redox signaling in cells.<sup>39</sup> As shown in Fig. 3(D), the intracellular ROS (expressed as % vs. control) decreased significantly in a dose-dependent manner in cells treated for 24 h with the DSeU@ZIF8 particles, whereas this effect was minimal when using the same doses of the free DSeU. In addition, different incubation times were also studied (1 h, 4 h, 6 h and 24 h, Fig. S20, ESI†) revealing that no or quite low effects were observed at short incubation times (1 h and 4 h), most likely due to a low internalization rate of the particles. Increasing the incubation time, the effect increased as expected, so that 24 h of incubation was selected as the optimal for the following assays. It should be noted that ZIF8 particles used as control also presented some antioxidant activity (statistically significant; *p* > 0.01 vs. control) at the low concentrations used, Fig. 3(D). This finding may be associated with (i) the favorable chemisorption of peroxides on ZIF8 *via* π-anion

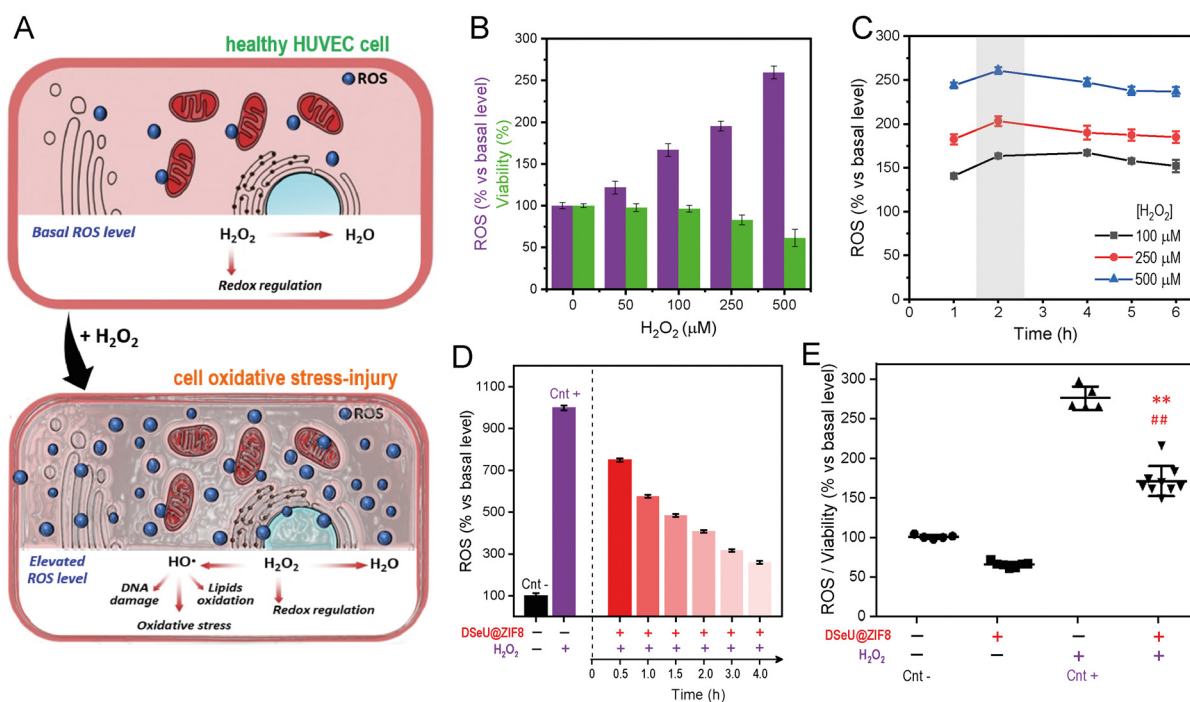


Fig. 4 (A) *In vitro* model of oxidative stress-injury (H<sub>2</sub>O<sub>2</sub>-induced HUVEC cells). (B) Effect in HUVEC cells of H<sub>2</sub>O<sub>2</sub>-induced oxidative stress using concentrations from 50 to 500 μM for 2 h of treatment. Data are shown as mean ± SD, *n* = 3 independent replicates. (C) Evolution of ROS over time (from 1 h to 6 h) in cells treated with different H<sub>2</sub>O<sub>2</sub> concentrations. Data are shown as mean ± SD, *n* = 3 independent replicates. (D) Monitoring of the intracellular ROS scavenging activity by DSeU@ZIF8 particles over time. Cells were first incubated with DSeU@ZIF8 (1 μM, 24 h), followed by H<sub>2</sub>O<sub>2</sub> treatment (100 μM, 2 h) to induce oxidative-stress damage. The negative control corresponds to the basal ROS level in untreated cells, whereas the positive control is the ROS level after H<sub>2</sub>O<sub>2</sub> stimulation of cells. (E) ROS scavenging activity of DSeU@ZIF8 particles measured after 2 h from stimulation; data normalized against the number of viable cells. Data are shown as mean ± SD, *n* = 3 independent replicates. *p* value < 0.05 was considered statistically significant; \*\**p* < 0.01 vs. negative control, and ##*p* < 0.01 vs. positive control.



stacking interactions between the peroxide nucleophiles and imidazole rings, as previously demonstrated by computational studies to explain the mechanism of some ZIF-catalyzed reactions involving  $\text{H}_2\text{O}_2$  as the oxidant reagent,<sup>40</sup> and/or (ii) the possible antioxidant and anti-inflammatory effect of  $\text{Zn}^{+2}$  ions released to cells from dissolution of ZIF8, resulting in either the potential activation of the antioxidant enzyme superoxide dismutase (SOD1 and 3, containing Zn and Cu in its active sites),<sup>41</sup> or decreasing the production of free radical by inhibition of the nicotinamide adenine dinucleotide phosphate (NADPH) oxidase.<sup>42</sup> Importantly, since the antioxidant function observed with DSeU@ZIF8 particles is superior compared to any of the individual components, presenting a fold-decrease of 1.55 (from 100% to 64.5%, once normalized the ROS level against cell viability, Fig. 3(E)), these results seem to indicate that there is a synergistic effect, which has also been reported for other MOF composites.<sup>31</sup>

To assess further whether the DSeU@ZIF8 particles were able to mitigate the negative effects caused by high ROS levels, *i.e.*, acting as an effective ROS-scavenger, we established first a cell model of oxidative stress-injury by treating HUVEC cells with  $\text{H}_2\text{O}_2$  (denoted as  $\text{H}_2\text{O}_2$ -induced HUVEC, Fig. 4(A)). It should be noted that  $\text{H}_2\text{O}_2$  was selected as model ROS molecule because it is typically generated at higher concentrations than other ROS; indeed, it is considered the most important ROS with regards to mitogenic stimulation or cell cycle regulation.<sup>43</sup>

Moreover,  $\text{H}_2\text{O}_2$  has a relatively long half-life, good membrane permeability, ensuring thus significant and dose-dependent intracellular concentrations. Using previous studies as reference,<sup>44</sup>  $\text{H}_2\text{O}_2$  concentrations ranging from 50 to 500  $\mu\text{M}$  and treatment times from 1 h to 6 h were studied. ROS and WST-1 assays were used to select the appropriate concentration of  $\text{H}_2\text{O}_2$  and incubation period. Bearing in mind that the ROS assay is strongly influenced by the number of viable cells, in the case that cell viability could be affected after treatments, data of fluorescence intensity (derived from ROS assay) have to be normalized against cell viability. As shown in Fig. 4(B), the ROS activity in cells increased in a dose-dependent manner after treatment with increasing concentrations of  $\text{H}_2\text{O}_2$ , whereas the influence of the incubation time was much less, observing the maximum effect after 2 h of treatment (Fig. 4(C)). Similarly, the cell viability also showed a dose-dependent response, decreasing significantly when the  $\text{H}_2\text{O}_2$  concentration was increased to 250  $\mu\text{M}$ . With a 100  $\mu\text{M}$  treatment for 2 h, HUVEC cells increased their intracellular ROS level but without compromising their viability (94%), so that these conditions were selected to establish the  $\text{H}_2\text{O}_2$ -induced HUVEC cell model. As shown in Fig. 4(D), cells treated with  $\text{H}_2\text{O}_2$  (at the fixed concentration 100  $\mu\text{M}$  for 2 h) resulted in a 9.9-fold enhancement of intracellular ROS compared to control cells. However, when cells were pre-treated with DSeU@ZIF8 particles (1  $\mu\text{M}$ , 24 h) before  $\text{H}_2\text{O}_2$  stimulation, the ROS generated initially (measured after 30 min of finishing the  $\text{H}_2\text{O}_2$

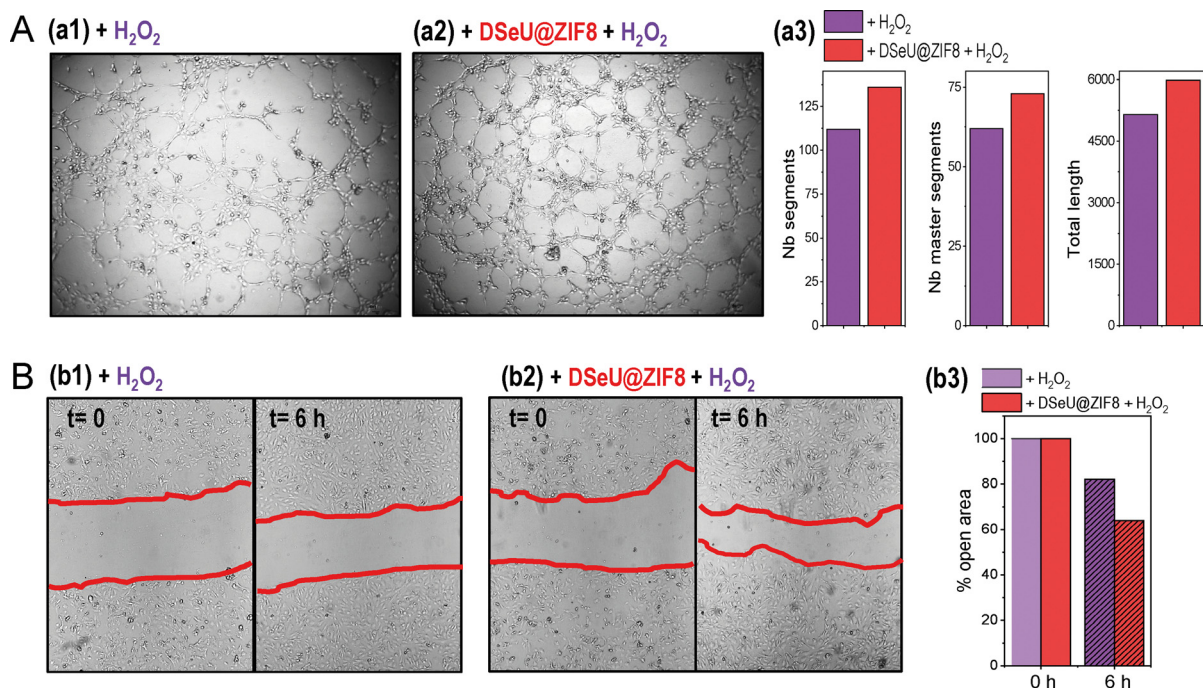


**Fig. 5** (A) Representative optical microscopy images of the formation of vessels in the *in vitro* angiogenesis assay on the semi-natural matrix 3D matrix (matrigel, 2 h after seeding) after the treatment of HUVECs with: (a1)  $\text{H}_2\text{O}_2$  (100  $\mu\text{M}$ , 2 h) used as a positive control, and (a2) cells incubated first with DSeU@ZIF8 particles (1  $\mu\text{M}$ , 24 h), followed by exposure to  $\text{H}_2\text{O}_2$  (100  $\mu\text{M}$ , 2 h); (a3) tube formation was evaluated by measurement of the number (Nb) of segments, Nb master segments and total length of vessels under each condition is shown. (B) Wound healing assay in HUVECs monolayers, showing the representative optical microscopy images of the wound at different times (extent of the wound marked with red lines) under different treatments as indicated (b1 and b2, the same as those used in the angiogenesis assay); (b3) Change in the size of the remaining wound after 6 h (represented as % open area vs. the initial damage).



stimulation) was significantly lower than in the absence of the particles. Representative images of inverted optical microscopy of HUVEC cells after these different treatments are shown in Fig. S21 (ESI<sup>†</sup>). More importantly, the level of ROS decreased even more with time as the particles were performing their function, reaching a 3.8-fold decrease after 4 h from the stimulation. The same conclusion is drawn from the ROS data normalized against the number of viable cells (Fig. 4(E)).

Going a step further we investigated the effect of H<sub>2</sub>O<sub>2</sub>-induced oxidative stress on different processes related to endothelial damage, such as angiogenesis and migration in mature endothelial cells, as well as the possibility of alleviating such negative impact by treating cells with the here designed ROS-scavenging DSeU@ZIF8 particles. Note that increased oxidative stress has been linked to impaired endothelial function and seems to play a role in the pathogenesis of many diseases, including cardiovascular and inflammatory diseases.<sup>45</sup> Therefore, in addition to evaluating the ROS-scavenging potential of new designed nanomaterials, their effect on the endothelial functions should be also considered (see ESI<sup>†</sup> for details). As shown in Fig. 5(A), the exposure of cells to H<sub>2</sub>O<sub>2</sub> affected negatively to their capacity to form new vessels in the 3D matrix, resulting in an inhibition of *in vitro* angiogenesis. However, cells pretreated with DSeU@ZIF8 better preserved their angiogenesis activity after being subjected to the same oxidative stress conditions, as derived from the higher number of Nb segments and Nb master segments as well as the greater total length of vessels in those HUVECs containing the DSeU@ZIF8 particles. Likewise, H<sub>2</sub>O<sub>2</sub> exhibited a deleterious effect on HUVECs proliferation decreasing its capacity to repair the endothelium, but the presence of DSeU@ZIF8 inside cells notably accelerated the wound healing process (Fig. 5(B)). Taken together, these results suggest that DSeU@ZIF8 particles are able to counteract the endothelial damage induced by H<sub>2</sub>O<sub>2</sub>, demonstrating again their ROS-scavenging activity in cells, and their subsequent impact on the protection of the endothelium functions.

## Conclusions

We have reported for the first time the successful incorporation of Se-containing sp<sup>2</sup>-IGLs into ZIF8 nanostructures and demonstrated the performance of the as-designed nanoparticles as antioxidant and ROS-scavenging nanoplatfoms in living cells. The presented results clearly showed the efficiency of the DSeU@ZIF8 nanoparticles in modulating the basal ROS level, and their capacity to mitigate the negative effect caused by H<sub>2</sub>O<sub>2</sub>-induced damage in cells. The beneficial effects of DSeU@ZIF8 particles on preserving critical functions of endothelial cells (*i.e.*, angiogenesis and cell migration) by reducing oxidative stress through removal of ROS, and increasing the endogenous enzyme activities have also been demonstrated. Further studies with different bioactive sp<sup>2</sup>-IGLs to expand the scope of the synthetic methodology to finally widen the therapeutic window of GlycoZIF-based nanoplatfoms are currently being developed in our laboratories.

## Author contributions

Conceptualization, C. C.-C.; methodology, C. C.-C., F. G. and E. M. S.-F.; investigation, C. C.-C., F. G., A. C., V. V., A. F. and E. M. S.-F.; formal analysis: F. G. and C. C.-C. writing – original draft, C. C.-C.; writing – review & editing, E. M. S.-F., F. G., A. M. M., and C. C.-C.; supervision, C. C.-C.; funding acquisition, C. C.-C., F. G., A. M. M. and E. M. S.-F. All authors have discussed the results and given approval to the manuscript.

## Conflicts of interest

There are no conflicts to declare.

## Acknowledgements

This work was supported by grants from the Spanish Ministry of Science, Innovation and Universities and the Spanish Research Agency (RYC-2019-027527-I and PID2022-141034OB-C22 to C. C.-C., PID2019-105858RB-I00 and PID2022-141034OB-C21 to E. M. S.-F.) and from the Junta de Andalucía (CSyF 2022 project, PI-0130-2022 to F. G. and A.M.-M.). Financial support was also provided from the University of Seville (VIPIT-2020-IV.2 to C. C.-C., and VIIPIT-2022-V.1 Modality A2 to E. M. S.-F. and C. C.-C.). The authors are grateful to Dra. García Jurado from IMIBIC Microscopy Unit for her technical assistance. Technical assistance from the research support services of the University of Seville (CITIUS) is also acknowledged.

## References

- H. J. Shields, A. Traa and J. M. Van Raamsdonk, *Front. Cell Dev. Biol.*, 2021, **9**, 628157.
- S. Reuter, S. C. Gupta, M. M. Chaturvedi and B. B. Aggarwal, *Free Radical Biol. Med.*, 2010, **49**, 1603.
- (a) J. Zhang, X. Wang, V. Vikash, Q. Ye, D. Wu, Y. Liu and W. Dong, *Oxid. Med. Cell. Longevity*, 2016, **2016**, 4350965; (b) Z. Li, X. Xu, X. Leng, M. He, J. Wang, S. Cheng and H. Wu, *Arch. Virol.*, 2017, **162**, 603; (c) J. Checa and J. M. Aran, *J. Inflamm. Res.*, 2020, **13**, 1057.
- J. Pei, X. Pan, G. Wei and Y. Hua, *Front. Pharmacol.*, 2023, **14**, 1147414.
- H. J. Reich and R. J. Hondal, *ACS Chem. Biol.*, 2016, **11**, 821.
- P. A. Nogara, M. E. Pereira, C. S. Oliveira, L. Orian and J. B. T. Rocha, *New J. Chem.*, 2023, **47**, 9959.
- (a) T. Li and H. Xu, *Cell Rep. Phys. Sci.*, 2020, **1**, 100111; (b) A. Khurana, S. Tekula, M. A. Saifi, P. Venkatesh and C. Godugu, *Biomed. Pharmacother.*, 2019, **111**, 802.
- (a) W. Hou and H. Xu, *J. Med. Chem.*, 2022, **65**, 4436; (b) F. Mangiavacchi, I. F. Coelho Dias, I. Di Lorenzo, P. Grzes, M. Palomba, O. Rosati, L. Bagnoli, F. Marini, C. Santi, E. Joao Lenardao and L. Sancineto, *Pharmaceuticals*, 2020, **13**, 211.
- T. Schewe, *Gen. Pharmacol.*, 1995, **26**, 1153.
- K. Bijian, Z. Zhang, B. Xu, S. Jie, B. Chen, S. Wan, J. Wu, T. Jiang and M. A. Alaoui-Jamali, *Eur. J. Med. Chem.*, 2012, **45**, 143.



- 11 (a) J. G. Fernández-Bolaños, Ó. López, V. Ulgar, I. Maya and J. Fuentes, *Tetrahedron Lett.*, 2004, **45**, 4081; (b) T. Manna and A. Kumar Misra, *Org. Biomol. Chem.*, 2019, **17**, 8902.
- 12 E. M. Sánchez-Fernández, R. García-Hernández, F. Gamarro, A. I. Arroba, M. Aguilar-Diosdado, J. M. Padrón, J. M. García Fernández and C. Ortiz Mellet, *Molecules*, 2021, **26**, 7501.
- 13 J. M. García Fernández, C. Ortiz Mellet, M. González-Cuesta, E. M. Sánchez-Fernández, Y.-J. Chang and A. Chuan-Ying Lai, EP21382981.5, 2021. PCT/EP2022/079912, 2022.
- 14 V. M. Díaz Pérez, M. I. García Moreno, C. Ortiz Mellet, J. Fuentes, J. C. Díaz Arribas, F. J. Cañada and J. M. García Fernández, *J. Org. Chem.*, 2000, **65**, 136.
- 15 (a) E. M. Sánchez-Fernández, R. Rísquez-Cuadro, M. Chasseraud, A. Ahidouch, C. Ortiz Mellet, H. Ouadid-Ahidouch and J. M. García Fernández, *Chem. Commun.*, 2010, **46**, 5328; (b) E. M. Sánchez-Fernández, M. I. García-Moreno, A. I. Arroba, M. Aguilar-Diosdado, J. M. Padrón, R. García-Hernández, F. Gamarro, S. Fustero, J.-E. Sánchez-Aparicio, L. Masgrau, J. M. García Fernández and C. Ortiz Mellet, *Eur. J. Med. Chem.*, 2019, **182**, 111604.
- 16 E. M. Sánchez-Fernández, M. I. García-Moreno, J. M. García Fernández and C. Ortiz Mellet, in *sp<sup>2</sup>-Iminosugars as Chemical Mimics for Glycodrug Design*, ed. A. Trabocchi and E. Lenci, Elsevier, 2020, pp.197–224.
- 17 T. S. Leyane, S. W. Jere and N. N. Houreld, *Int. J. Mol. Sci.*, 2022, **23**, 7273.
- 18 E. M. Sánchez-Fernández, M. I. García-Moreno, R. García-Hernández, J. M. Padrón, J. M. García Fernández, F. Gamarro and C. Ortiz Mellet, *Molecules*, 2019, **24**, 2882.
- 19 F. Cano-Cano, E. Alcalde-Estévez, L. Gómez-Jaramillo, M. Iturregui, E. M. Sánchez-Fernández, J. M. García Fernández, C. Ortiz Mellet, A. Campos-Caro, C. López-Tinoco, M. Aguilar-Diosdado, A. M. Valverde and A. I. Arroba, *Front. Immunol.*, 2021, **12**, 632132.
- 20 L. Gómez-Jaramillo, F. Cano-Cano, E. M. Sánchez-Fernández, C. Ortiz Mellet, J. M. García-Fernández, M. Alcalá, F. Álvarez-Gallego, M. Iturregui, M. C. González-Montelongo, A. Campos-Caro, A. I. Arroba and M. Aguilar-Diosdado, *Int. J. Mol. Sci.*, 2022, **23**, 8450.
- 21 E. Schaeffer, E. M. Sánchez-Fernández, R. Gonçalves-Pereira, V. Flacher, D. Lamon, M. Duval, J.-D. Fauny, J. M. García Fernández, C. G. Mueller and C. Ortiz Mellet, *Eur. J. Med. Chem.*, 2019, **169**, 111.
- 22 (a) S. R. Batten, N. R. Champness, X.-M. Chen, J. García-Martínez, S. Kitagawa, L. Öhrström, M. O’Keeffe, M. P. Suh and J. Reedijk, *Pure Appl. Chem.*, 2013, **85**, 1715; (b) H. Furukawa, K. E. Cordova, M. O’Keeffe and O. M. Yaghi, *Science*, 2013, **341**, 1230444.
- 23 (a) P. Horcajada, R. Gref, T. Baati, P. K. Allan, G. Maurin, P. Couvreur, G. Férey, R. E. Morris and C. Serre, *Chem. Rev.*, 2012, **112**, 1232; (b) T. Simon-Yarza, A. Mielcarek, P. Couvreur and C. Serre, *Adv. Mater.*, 2018, **30**, e1707365.
- 24 C. R. Marshall, S. A. Staudhammer and C. K. Brozek, *Chem. Sci.*, 2019, **10**, 9396.
- 25 L. Feng, G. S. Day, K. Y. Wang, S. Yuan and H. C. Zhou, *Chem*, 2020, **6**, 2902.
- 26 C. V. McGuire and R. S. Forgan, *Chem. Commun.*, 2015, **51**, 5199.
- 27 M. D. J. Velásquez-Hernández, R. Ricco, R. Carraro, F. T. Limpoco, M. Linares-Moreau, E. Leitner, H. Wiltzsche, J. Rattenberger, H. Schröttner, P. Frühwirt, E. M. Stadler, G. Gescheidt, H. Amenitsch, C. J. Doonan and P. Falcaro, *CrystEngComm*, 2019, **21**, 4538.
- 28 (a) K. Liang, R. Ricco, C. M. Doherty, M. J. Styles, S. Bell, N. Kirby, S. Mudie, D. Haylock, A. J. Hill, C. J. Doonan and P. Falcaro, *Nat. Commun.*, 2015, **6**, 7240; (b) F.-K. Shieh, S. C. Wang, C.-I. Yen, C.-C. Wu, S. Dutta, L. Y. Chou, J. V. Morabito, P. Hu, M.-H. Hsu, K.-W. Wu and C. K. Tsung, *J. Am. Chem. Soc.*, 2015, **137**, 4276; (c) F. Carraro, M. D. J. Velásquez-Hernández, E. Astria, W. Liang, L. Twilight, C. Parise, M. Ge, Z. Huang, R. Ricco, X. Zou, L. Villanova, C. O. Kappe, C. Doonan and P. Falcaro, *Chem. Sci.*, 2020, **11**, 3397; (d) M. D. J. Velásquez-Hernández, M. Linares-Moreau, E. Astria, F. Carraro, M. Z. Alyami, N. M. Khashab, C. J. Sumby, C. J. Doonan and P. Falcaro, *Coord. Chem. Rev.*, 2021, **429**, 213651.
- 29 (a) K. Liang, R. Wang, M. Boutter, C. M. Doherty, X. Muleta and J. J. Richardson, *Chem. Commun.*, 2017, **53**, 1249; (b) R. E. Giménez, E. Piccinini, O. Azzaroni and M. Rafti, *ACS Omega*, 2019, **4**, 842.
- 30 (a) R. A. Smaldone, R. S. Forgan, H. Furukawa, J. J. Gassensmith, A. M. Z. Slawin, O. M. Yaghi and J. F. Stoddart, *Angew. Chem., Int. Ed.*, 2010, **49**, 8630; (b) K. Krukler-Berzin, S. Belyakov, A. Mishnev and K. Shubin, *Crystals*, 2020, **10**, 37.
- 31 M. D. J. Velásquez-Hernández, E. Astria, S. Winkler, W. Liang, H. Wiltzsche, A. Poddar, R. Shukla, G. Prestwich, J. Paderi, P. Salcedo-Abraira, H. Amenitsch, P. Horcajada, C. J. Doonan and P. Falcaro, *Chem. Sci.*, 2020, **11**, 10835.
- 32 G. Calvo-Martín, D. Plano, I. Encío and C. Sanmartín, *Antioxidants*, 2021, **10**, 777.
- 33 (a) M. Koketsu, N. Takakura and H. Ishihara, *Synth. Commun.*, 2002, **32**, 3075; (b) H. Ishihara, M. Koketsu, Y. Fukuta and F. Nada, *J. Am. Chem. Soc.*, 2001, **123**, 8408.
- 34 Y. Pan, D. Heryadi, F. Zhou, L. Zhao, G. Lestari, H. Su and Z. Lai, *CrystEngComm*, 2011, **13**, 6937.
- 35 S. Behzadi, V. Serpooshan, W. Tao, M. A. Hamaly, M. Y. Alkawareek, E. C. Dreaden, D. Brown, A. M. Alkilany, O. C. Farokhzad and M. Mahmoudi, *Chem. Soc. Rev.*, 2017, **46**, 4218.
- 36 S. Gao, J. Hou, Z. Deng, T. Wang, S. Beyer, A. Guilherme Buzanich, J. J. Richardson, A. Rawal, R. Seidel, M. Yazid Zulkifli, W. Li, T. D. Bennett, A. K. Cheetham, K. Liang and V. Chen, *Chem*, 2019, **5**, 1597.
- 37 L. Palanikumar, S. Al-Hosani, M. Kalmouni, V. P. Nguyen, L. Ali, R. Pasricha, F. N. Barrera and M. Magzoub, *Commun. Biol.*, 2020, **3**, 95.
- 38 T. Hidalgo, R. Simón-Vázquez, A. González-Fernández and P. Horcajada, *Chem. Sci.*, 2022, **13**, 934.
- 39 L. Milkovic, A. Cipak Gasparovic, M. Cindric, P.-A. Mouthuy and N. Zarkovic, *Cells*, 2019, **8**, 793.



- 40 A. Franco, A. Negi, R. Luque and C. Carrillo-Carrión, *ACS Sustainable Chem. Eng.*, 2021, **9**, 8090.
- 41 Y. Song, S. W. Leonard, M. G. Traber and E. Ho, *J. Nutr.*, 2009, **139**, 1626.
- 42 S. Prasad, *Curr. Opin. Clin. Nutr.*, 2009, **12**, 646.
- 43 G. P. Bienert, J. K. Schjoerring and T. P. Jahn, *Biochim. Biophys. Acta*, 2006, **1758**, 994.
- 44 G. Wang, M. Hao, Q. Liu, Y. Jiang, H. Huang, G. Yang and C. Wang, *J. Zhejiang Univ., Sci., B*, 2021, **22**, 348.
- 45 (a) N. Edwards, A. W. Langford-Smith, F. L. Wilkinson and M. Y. Alexander, *Front. Med.*, 2018, **5**, 200; (b) S. Shafi, H. R. Ansari, W. Bahitham and S. Aouabdi, *Front. Cardiovasc. Med.*, 2019, **6**, 28.

